Journal Pre-proof

Reliability of an injection-moulded two-piece zirconia implant with PEKK abutment after long-term thermo-mechanical loading

Fei Zhang, Christoph Meyer zur Heide, Jérome Chevalier, Jozef Vleugels, Bart Van Meerbeek, Christian Wesemann, Bernardo Camargo dos Santos, Valter Sergo, Ralf-Joachim Kohal, Erik Adolfsson, Insa Herklotz, Benedikt C. Spies

PII: S1751-6161(20)30520-8

DOI: https://doi.org/10.1016/j.jmbbm.2020.103967

Reference: JMBBM 103967

To appear in: *Journal of the Mechanical Behavior of Biomedical Materials*

Received Date: 11 May 2020

Revised Date: 29 June 2020

Accepted Date: 1 July 2020

Please cite this article as: Zhang, F., Meyer zur Heide, C., Chevalier, Jé., Vleugels, J., Van Meerbeek, B., Wesemann, C., Camargo dos Santos, B., Sergo, V., Kohal, R.-J., Adolfsson, E., Herklotz, I., Spies, B.C., Reliability of an injection-moulded two-piece zirconia implant with PEKK abutment after long-term thermo-mechanical loading, *Journal of the Mechanical Behavior of Biomedical Materials* (2020), doi: https://doi.org/10.1016/j.jmbbm.2020.103967.

Fei Zhang: Formal analysis; Investigation; Methodology; Funding acquisition; Visualization; Writing - original draft; Writing - review & editing. **Christoph Meyer zur Heide:** Investigation; Writing - original draft. **Jérome Chevalier:** Formal analysis; Funding acquisition; Methodology; Writing - review & editing. **Jozef Vleugels:** Formal analysis; Methodology; Supervision; Writing - review & editing. **Christian Wesemann:** Investigation; Formal analysis. **Bernardo Camargo dos Santos:** Investigation; Writing - original draft; **Bart Van Meerbeek:** Supervision; Writing - review & editing. **Valter Sergo:** Funding acquisition; Writing - review & editing. **Kohal Ralf-Joachim:** Methodology; Writing - review & editing. **Erik Adolfsson:** Funding acquisition; Writing - review & editing. **Insa Herklotz:** Investigation (Clinical Failure). **Spies Benedikt:** Formal analysis; Investigation; Methodology; Supervision; Funding acquisition; Visualization; Writing - original draft; Writing - review & editing.

Reliability of an injection-moulded two-piece zirconia implant with PEKK abutment after long-term thermo-mechanical loading

Fei Zhang[ab]*[#], Christoph Meyer zur Heide[c]*[¶], Jérome Chevalier[d], Jozef Vleugels[b], Bart Van Meerbeek[a], Christian Wesemann[c], Bernardo Camargo dos Santos[a], Valter Sergo[e,g], Ralf-Joachim Kohal[f], Erik Adolfsson[h], Insa Herklotz[c], Benedikt C. Spies[c]

a. KU Leuven (University of Leuven), Department of Oral Health Sciences, BIOMAT - Biomaterials Research group & UZ Leuven (University Hospitals Leuven), Dentistry, Kapucijnenvoer 7 blok a, B-3000 Leuven, Belgium

b. KU Leuven, Department of Materials Engineering, Kasteelpark Arenberg 44, B-3001 Heverlee, Belgium

c. Charité - Universitätsmedizin Berlin, corporate member of Freie Universität Berlin, Humboldt-Universität zu Berlin, and Berlin Institute of Health, Department of Prosthodontics, Geriatric Dentistry and Craniomandibular Disorders, Aßmannshauser Str. 4-6, Berlin, Germany

d. Université de Lyon, INSA-Lyon, UMR CNRS 5510 MATEIS, 20 Avenue Albert Einstein, 69621 Villeurbanne Cedex, France

e. Engineering and Architecture Dept., University of Trieste, Italy

f. Medical Center – University of Freiburg, Center for Dental Medicine, Department of Prosthetic Dentistry, Faculty of Medicine, University of Freiburg, Hugstetter Str. 55, 79106 Freiburg, Germany

g. Faculty of Health Sciences, University of Macau, Macau SAR, China

h. RISE AB, Argongatan 30, 431 53 Mölndal, Sweden

*Equal first author contribution

[#] Corresponding author: Fei Zhang, KU Leuven (University of Leuven), Department of Oral Health Sciences, BIOMAT -Biomaterials Research group & UZ Leuven (University Hospitals Leuven), Dentistry, Kapucijnenvoer 7 blok a, B-3000 Leuven, Belgium

Email address: fei.zhang@kuleuven.be

[¶]Full length name: Meyer zur Heide genannt Meyer-Arend, Christoph Ernst Johannes

Abstract

Zirconia implants are appreciated in some clinical indications in light of their aesthetic appearance and good biocompatibility. The aim of this work was to evaluate the performance of a newly developed two-piece zirconia/polyether ketone ketone (PEKK) implant-abutment combination after long-term cyclic loading in a hydrothermal environment, using a new protocol adapted from two available ISO standards. Sixteen implants (n=8/group) were embedded according to ISO 14801 and divided into two groups: implants in the Observational Group (OG) were cyclically loaded for 60 days (98 N, 10 million loading cycles, 2 Hz) in 85°C water in a chewing simulator, while non-loaded/non-aged implants (as-received) constituted the Control Group (CG). After 4.7 million loading cycles, one OG implant fractured in the chewing simulator. The surviving implants were compared to CG implants by X-ray diffraction (XRD) to investigate potential ageing as suggested by ISO 13356, but also µ-Raman spectroscopy, Focused-Ion-Beam - Scanning-Electron-Microscopy (FIB-SEM), and load-to-fracture. Ageing was shown to have limited influence on the evaluated zirconia implant, with increased monoclinic content after loading/ageing being to a shallow transformed zone of ~2 µm at the implant surface. However, OG implants showed a significantly decreased fracture load of 751 ± 231 N (CG: 995 ± 161 N; p=.046). These values enable clinical application, but the fact that one failure was recorded during cyclic fatigue

along with the significant decrease in strength after cyclic loading/ageing suggest that there may be room for further optimization of especially the PEKK abutment. Furthermore, good agreement was observed between the fracture modes of the implant that failed during the cyclic fatigue experiment and the *in vivo* failure of one implant during pre-clinical trials, validating the interest of the *in vitro* protocol used in this work to check the reliability of zirconia implant.

Keywords: Zirconia; Two-piece implants; Fatigue; Ageing; PEKK

1. Introduction

Already 50 years ago, intra-osseous oral implants made from commercially pure titanium were successfully inserted in dogs and later on in humans [1]. To the present date, titanium implants represent a well-documented and widely established treatment option for both fixed dental prostheses as well as removable dentures [2, 3]. Although ceramic implants made from aluminium oxide have been developed and investigated during the same period [4, 5], they did not really penetrate the market [6, 7], with their lower mechanical resistance being considered as potential reason [8] and the fact that the high stiffness of alumina ceramics (E-modulus of about 330 GPa) is more likely to cause bone resorption through stress shielding. The introduction of high-strength zirconia ceramics with a lower stiffness (E-modulus of about 210 GPa) in dentistry along with the rising aesthetic demands from patients have recently renewed the research & development interest in ceramic implants and their market share [7]. Clinical trials and animal studies have shown that zirconia implants show similar osseointegration compared to titanium implants [9-11]. Furthermore, zirconia ceramics present an excellent biocompatibility in terms of reduced bacterial adhesion, biofilm and plaque accumulation [12, 13]. Amongst different types of zirconia(-based) ceramics, 3 mol%

yttria-stabilized tetragonal zirconia polycrystals (3Y-TZP), revealing a flexural strength of ~1000 MPa and fracture toughness of 5–10 $MPa \cdot m^{1/2}$ due to a phase-transformation toughening (PTT) mechanism, are currently considered as the standard material for manufacturing ceramic dental implants [14]. However, Y-TZP ceramics may undergo a slow phase-transformation in an aqueous environment (often referred as low-temperature degradation [LTD] or hydrothermal ageing), potentially leading to micro-cracking, surface roughening and in the worst cases to a premature fracture of the ceramic object [15, 16].

Most of the presently available zirconia implant systems are manufactured in a subtractive manner by machining and grinding in a fully sintered and hipped (Hot Isostatic Pressing [HIP]) condition or in a pre-sintered stage [17-19]. Although highly precise and fatigue-resistant products can be obtained [20, 21], in addition to the high tooling costs, subsequent post-processing such as sandblasting, acid etching, laser treatment, etc. [18, 22] is necessary to achieve a micro-rough surface in enhancement of osseointegration. On the other hand, ceramic injection moulding (CIM) using a ceramic feedstock that is injected into prefabricated moulds can directly shape and roughen the implant with sufficient precision and fracture resistance [22, 23], resulting in reduced production cost, tool wear and less powder waste.

Currently available zirconia implants demonstrating mid-term clinical success are monoblocs comprising both the endosseous part and abutment in a single piece. Such a one-piece design can be beneficial as it lacks potential stress concentration at the interface and at the screw attachment, and also avoiding the implant-abutment gap which can be prone to bacterial colonisation. Moreover, a one-piece design avoids multiple fragile components, thereby exposing a reduced total surface area to environmental conditions [7]. However, one-piece implants reveal a limited clinical indication range and are challenging for both the surgeon and prosthodontist. Therefore and to answer clinical demands, several two-piece zirconia

implant systems have recently entered the market [7, 20, 24, 25]. Long-term clinical data is still missing [26] and different material combinations for the implant abutment (zirconia, PEEK, PEKK, glas-fiber) and abutment screw (titanium, gold, zirconia, carbon-fiber reinforced PEEK) are developed. The combination studied in this work was a commercial available system comprising a zirconia implant with Polyether Ketone Ketone (PEKK) abutment, and this was very recently developed by a company. In addition to the interest from zirconia ceramic, PEKK as a high-performance polymer from the Polyaryl Ether Ketone (PAEK) family is also new and interesting for dental application due to its natural looking, radiolucency and biocompatibility [27, 28].

The purpose of the present investigation was to investigate the long-term reliability of this zirconia-PEKK combination. In particular, the study's focus was the zirconia implant body, because it was considered that the risk of potential failure/degradation may originate from the ceramic part. For this purpose, a study protocol including an ageing and cyclic fatigue procedure developed for zirconia implants was applied [29]. Two international ISO standards were used and combined to address the clinical safety and long-term stability of these implants. ISO 14801, mostly dedicated to titanium-based implants, prescribes an experimental setup for a dynamic fatigue procedure [30]. It demands to test the final market-ready product by cyclic fatigue with an angulation of 30° to the vertical axis along with a simulated alveolar bone recession of 3 mm. Other environmental factors like ageing or horizontal forces to simulate intraoral conditions to the extent possible are not considered. Furthermore, this ISO standard does not define any minimum requirements that finally need to be fulfilled. ISO 13356 examines zirconia test specimens subjected to humidity at 134°C and 0.2 MPa for 5 hours [31]. Instead of market-available products, standardized bending bars with a polished surface are evaluated. Since the manufacturing technique, the type of micro-roughening as well as the geometry are known to significantly influence strength and ageing kinetics [22, 32,

33], an alternative test protocol was proposed, namely measuring the mechanical resistance of zirconia implants subjected to artificial loading with simultaneous hydrothermal ageing [29]. The procedure consisted of long-term (10 million cycles) cyclic fatigue including horizontal forces and an ageing-inducing environment. For the implants that survived the fatigue process, the mechanical property was assessed by a load-to-fracture test.

2. Materials and Methods

2.1. Implant

The implants tested were screw-retained two-piece implants comprising a zirconia implant body with PEKK abutment (Fig. 1) that was recently developed by a company (Ceralog Hexalobe Implant, Axis biodental; Les Bois, Switzerland). The zirconia implant was manufactured by means of CIM followed by sintering, hipping and sterilization. The endosseous part had a cylindrical screw shape, measuring 4.0 mm in diameter and 12.0 mm in length, comprising surface roughening by the imprint of the mould without any further post-processed surface roughening. This implant type can be inserted epi- and supracrestally, so that the implant neck of 1.5 mm height is either positioned crestally or above. For the experiment, the supracrestal positioning of the implant was selected. The PEKK abutment consisted of a concave-shaped transgingival part, measuring 1.0 mm in height and a tapered part of 7.4 mm in height. The titanium abutment screws were tightened at 25 Ncm and re-tightened after 10 min.

2.2. Experimental setup

A total of 16 zirconia oral implants were included in the experiments and randomly assigned to two groups of eight samples each (Fig. 1). One group served as Observational Group (OG) and was subjected to cyclic loading and simultaneous hydrothermal treatment in a chewing simulator. The second group did not receive any treatment besides embedding and served as Control Group (CG) for all types of measurements. Phase composition and monoclinic phase content was quantified by XRD on a surface area of about 1x10 mm for all implants, whereas µ-Raman spectroscopy was complementarily used to locally resolve the monoclinic phase content at different spots with a lateral resolution of 4 µm (see Fig. 2 for the locations considered with both techniques). Finally, the subsurface microstructure and transformation depth was examined after FIB sectioning by SEM at three different spots of one representative CG implant and four different spots of one representative OG implant, respectively. Remaining (CG) and surviving (OG) implants were quasi-statically loaded to fracture in a universal testing machine and statistically analysed (n = 7/group with all OG implants surviving the cyclic fatigue procedure).

2.3. Embedding procedure

The embedding procedure was performed in accordance to ISO 14801. All implants were inserted in a dual-cure acrylic resin (LuxaCore Dual, DMG; Hamburg, Germany), simulating a bony recession of 3 mm which leads to 4.5 mm exposed implant length. The embedding resin had a modulus of elasticity of ~8 GPa which meets the requirements of ISO 14801 (>3 GPa) and furthermore approximates that of human bone [34] in order to be clinically relevant. The use of a custom-made external fixation device allowed an exact perpendicular embedding of all implants. Customized hemispheres were mounted on the abutments using a self-adhesive composite cement (RelyX Unicem, 3M Oral Care; Seefeld, Germany) to ensure

equal loading of the implants. The application of force during cyclic fatigue and the load-to-fracture test was exerted at an angle of 30° to the vertical axis using tilted sample holders. More details on the procedure can be found elsewhere [25, 29].

2.4. Cyclic loading and hydrothermal treatment

Fatigue of OG implants was performed using a computer-controlled dual-axis chewing simulator (CS-4.8, SD Mechatronik; Feldkirchen-Westerham, Germany) with eight chambers in water at 85°C. Each simulated chewing cycle included a downward vertical movement, a horizontal movement (chewing loading) and an upward vertical movement. A weight of 98 N (10 kg) was used for load application for 10 million cycles with a frequency of 2 Hz. In detail, each loading cycle consisted of the loading force being vertically applied to the highest point of the hemisphere of the angulated implant with a subsequent horizontal movement of 0.5 mm under the full load in the opposite direction of the inclination angle of the implant, representing occlusal pressure and horizontal shear during mastication. Due to the morphology of the alveolar bone, dental implants installed in the maxilla are mostly angulated to the buccal and implants installed in the (posterior) mandible angulated to the lingual. According to the commonly reported movement patterns during mastication in the frontal plane [35, 36], it can be assumed that contact glide in the closing masticatory stroke during mastication mainly occurs in the opposite direction of the inclination angle of the implant. Between two cycles the force was unloaded. The antagonist had a plane surface, and both antagonist and loading hemisphere were made of stainless steel. The loading frequency of 2 Hz was a result of the set operating parameters (horizontal movement of 0.5 mm at 30 mm/s, vertical movement of at 60 mm/s). More detailed configurations and operation modes of the chewing simulator were precisely described earlier [25].

Scientific data concerning the average *in vivo* chewing contacts are highly heterogeneous, ranging between 240,000 and 1,000,000 contacts per year [37-40]. As a consequence, 10 million loading cycles applied in this work might correspond to a considerably high range of 10–40 years of clinical use. Regarding the hydrothermal treatment, during the 60-day loading procedure, the sample chambers were heated and filled with water at a temperature set at 85°C to simultaneously simulate hydrothermal ageing during the loading procedure. According to the activation energy of the ageing reaction in zirconia ceramics [29, 41, 42], this hydrothermal treatment at 85°C for 60 days was estimated to correspond to roughly 40 years of ageing at a body temperature of 37°C [29].

2.5. Load-to-fracture test

With exception of one implant per group used for FIB-SEM (implants No. 1 and 9), all remaining (n = 7 CG implants) and surviving (n = 6 OG implants; one OG implant did not survive cyclic fatigue in the chewing simulator) samples were subsequently subjected to quasi-static loading to fracture using a universal testing machine (Zwick, Z010/TN2S; Ulm, Germany). A compressive load was likewise applied at an angle of 30° to the vertical under stroke control with a crosshead speed of 1 mm/min until failure occurred (fracture or sudden sharp drop of force curve in the recorded graph). Load-displacement curves were recorded for each implant.

2.6. Phase characterization

In order to analyse the effect of cyclic loading and ageing, XRD and µ-Raman were complementarily used to estimate the degree of phase transformation at the outer surface and at different locations, respectively. XRD was performed on the outer surface of implants with

an analysed area of about 1 mm in width and 10 mm in length, as indicated in Fig. 2. Penetration depth of the X-rays in zirconia is about 5–7 µm [43]. µ-Raman was used to characterize the phase composition at different positions along the external smooth and roughened surfaces (smooth transgingival part, thread root and thread crest) of the implants (Fig. 2). Depending on the experimental setup, including laser wavelength, objective magnification, numerical aperture of the lens, pinhole size, etc., the µ-Raman lateral spot size and sampling depth in zirconia ceramics are in the range of 1 to 4 µm and ~5 to 50 µm, respectively [44-46].

2.6.1. XRD

XRD (3003-TT, Seifert; Ahrensburg, Germany) was used to measure the monoclinic zirconia content at the surface of CG and OG implants before and after cyclic loading and hydrothermal treatment (n = 8/group). XRD patterns were collected in the 25–35° 2θ range with a step size of 0.02 for 2 s using a 2-mm slit size using CuK_α radiation at 40 kV and 40 mA. The monoclinic content (V_m) was calculated according to the formula of Garvie *et al.* [47] that was modified by Toraya *et al.* [48]:

$$V_m = \frac{1.311 \cdot X_m}{1 + 0.311 \cdot X_m} \quad (1)$$

$$X_m = \frac{I_{m(\bar{1}11)} + I_{m(111)}}{I_{m(\bar{1}11)} + I_{m(111)} + I_{t(101)}} \quad (2)$$

with X_m the integrated intensity ratio, $I_{m\ (h\ k\ l)}$ and $I_{t\ (h\ k\ l)}$ the area of the (hkl) peak of the monoclinic and tetragonal phase, respectively.

2.6.2. µ-Raman

µ-Raman spectra were collected using a 532 nm wavelength Ar-ion laser source of 20 mW through a 20x objective with a pinhole aperture of 25 µm in three successive measurements of 20 s integration time per measurement (Senterra, BrukerOptik; Ettlingen, Germany). Due to the geometry of the implants with thread root and crest, a higher magnification with smaller working distance could not be used. The µ-Raman configuration used in this work gave rise to a lateral analysis spot size of about 4 µm and 20 µm sampling depth below the surface [44, 45]. For each group, at least 50 spots were assessed for each position of the implant. The µ-Raman monoclinic zirconia fraction (V_m) was calculated according to the formula of Tabares *et al.* [49]:

$$V_m = \frac{I_m^{180} + I_m^{190}}{(I_m^{180} + I_m^{190}) + 0.32(I_t^{147} + I_t^{256})} \quad (3)$$

with I_m and I_t the integrated intensities of the monoclinic and tetragonal zirconia peaks, respectively. The integrated intensities were quantified on background-subtracted spectra using the built-in OPUS spectroscopy software.

2.7. FIB-SEM

FIB-SEM has been successfully used to examine the subsurface microstructure of zirconia implants and to determine the extent of the transformation zone and micro-crack formation [50, 51]. The surface microstructural characteristics of zirconia implants were preliminary observed using SEM and further evaluations of the implant subsurface were completed on FIB cross-sections. These experiments were performed using the FIB-SEM Nova NanoLab 600 DualBeam (FEI; Eindhoven, The Netherlands). The analysed samples were glued with silver paint onto an aluminium stub and were coated with a platinum layer of about 20 nm. To minimize the curtain effect introduced by gallium ion-beam milling and to protect the sample

surface from implantation, an *in-situ* ion beam-induced Pt deposition was performed over the areas of interest. Then, sections were milled to a depth that freed up a cross-sectional surface allowing assessing the phase transformations. Coarse milling of cross-sections in the size of about 30 µm width and 10–20 µm depth was performed at 30 kV ion accelerating voltage and 6.5 nA beam currents. Fine milling and cleaning were performed at 30 kV ion accelerating voltage and decreased beam currents from 2.7 nA, 0.9 nA, 0.44 nA till 0.26 nA in sequence to reach a suitable cross-section for SEM imaging and to avoid any ion-beam induced transformation. SEM imaging was performed at 2 kV simultaneously with secondary electron (SE) and energy filtered backscattered electron (BSE) imaging.

Three cross-sections were made for CG implants at positions analogous to those for µ-Raman analyses, i.e. smooth transgingival part, thread root and thread crest of the external roughened surface. For the dynamically loaded and aged OG implants, another implant was mechanically sectioned in half, upon which FIB-SEM was performed at the internal smooth surface in order to observe the influence of hydrothermal treatment on the internal implant structure.

The zirconia-grain size was measured on SEM micrographs according to the linear intercept method and a correction factor of 1.56 was applied to determine the real grain size [52].

2.8. X-ray tomography

X-ray tomography was conducted on the coronal and apical parts of the fractured implant to inspect the presence of residual porosities or large defects. Reconstruction into a digitized 3D image was made using a Phoenix Nanotom S (Baker Hughes; GE Sensing & Inspection Technology, Wunstorf, Germany). The X-ray tube was operated at 180 kV with a current of 145 µA and a 1.0-mm width copper filter. Three radiographic projections were obtained at a 0.15°-step interval with samples rotation of 360°, resulting in a total of 2400 projection angles

and scanning time of 40 minutes. The voxel size of current scanning was 3.66 µm, which in practice could allow the identification of defects on the order of 10 µm. Two-dimensional image projections were archived in 16 bit-TIFF and used for cross-sectional image reconstruction with phoenix datos|x v.2.6 software (Baker Hughes; GE Company LLC) followed by 3D evaluations using software packages CTAn v.1.14.4.1, Dataviewer and CTVox (Bruker Co.; Belgium).

2.9. Fractography

Fracture surfaces of all implants were examined by SEM (FEI-Nova Nanosem 450, FEI; Eindhoven, The Netherlands). The specimens were ultrasonically cleaned in ethanol before microscopic examination without any surface treatments nor conductive layer coating.

2.10. Statistical analyses

Levene tests were used to verify variance homogeneity of the results. Subsequently, pairwise Student's t-test for equal variances was performed to compare fracture load after load-to-fracture test, while unequal variances t-test (Welch-test) was used to analyse the XRD measurements. For µ-Raman spectroscopy measurements, a multivariate linear regression model with treatment (OG, CG implant group) and measurement position (smooth transgingival part, thread root and thread crest) as factors was applied. P-values and the effect size (partial eta squared [η^2]) were calculated. The level of significance for all tests was set at $p < .05$. The statistical analysis was performed with SPSS 22.0 (SPSS; Chicago, IL, USA).

3. Results

3.1. Cyclic fatigue and hydrothermal ageing test of OG implants

Seven of eight OG implants survived 10 million loading cycles with simultaneous hydrothermal ageing. One zirconia implant fractured after 4.7 million loading cycles (No. 14). After 6.5 million loading cycles, one abutment screw and the corresponding PEKK abutment fractured. In that latter case, both screw and abutment were replaced with the implant re-subjected to reach the target of 10 million loading cycles.

3.2. Load-to-fracture test

The fracture load values can be found in Table 1 and the failure probability plot in Figure 3 showing the data scattering. Due to one failure of the zirconia implant during cyclic fatigue, only 13 instead of 14 implants were available for the load-to-fracture test. Simultaneous cyclic loading and hydrothermal ageing of the implants significantly decreased the mean fracture load of the implant system from 995 ± 161 N to 751 ± 231 N ($p=0.046$). Note that Weibull modulus was not calculated because of the limited number of implants for each batch. However, OG implants revealed clearly increased scattering of the fracture load values. The maximum values were 1274 N for CG implants and 1033 N for OG implants, whereas minimum values of 799 N (CG) and 493 N (OG) were measured. Furthermore, the load versus displacement curve of OG implants with a stronger non-linearity revealed systematic higher deformation compared to CG implants (Fig. 4). Increased distortion of the abutments of the OG implants was also observed during the load-to-fracture process (see Appendix for slow-motion videos recording the fracture process).

3.3. Fractography

Fracture of all investigated zirconia-PEKK combinations occurred at the zirconia implant level with no fracture of the PEKK abutment or the Ti abutment screw. However, fracture initiation occurred at different locations of the implant body for CG and OG groups (Fig. 5). For all CG implants, the tip of the Ti abutment screw was exposed due to fracture, with crack initiation at the inner surfaces from the internal thread at the implant-abutment interface (Fig. 5a); micro-cracks, probably generated due to stress concentration along the implant-abutment interface, were observed. In all OG implants (Fig. 5b), fractures likewise occurred at the zirconia implant level. However, no exposure of the Ti abutment screw was observed and cracks initiated at the outer zirconia-implant surface, i.e. the roughened endosseous surface. Fracture mode of the implant failed during cyclic fatigue (Fig. 5c; n = 1, implant No. 14), probably initiated from the implant bulk, appeared to be significantly different compared to the fracture modes shown in Fig. 5b and c for OG and CG implants that survived the cyclic fatigue. However, the cause of fracture for this implant was not clearly identified.

3.4. Phase characterization by XRD and µ-Raman

The quantified monoclinic ZrO_2 phase content before (CG group) and after dynamic fatigue with cyclic loading and ageing (OG group) are shown in Table 2. XRD results showed that the monoclinic phase content on the outer surfaces of different specimens within each group had small deviation, even though the measurements were done on the micro-roughened surface. The surface monoclinic phase content on the OG implants was significantly higher compared to that on the CG implants (36 vol% versus 13 vol%; $p < .001$).

The locally resolved analyses at three positions by µ-Raman are shown in the boxplots in Fig. 6. The statistical analyses (Table 2) revealed that the distribution of monoclinic phase was not significantly influenced by the different locations of the implants ($p=.931$, $\eta^2=.001$). In

agreement with the XRD results and as expected, the combination of cyclic loading and ageing increased the surface monoclinic ZrO_2-phase content (~7 vol% on CG implants versus 2-4 vol% on OG implants; $p<.001$, $\eta^2=.145$).

3.5. Microstructure by FIB-SEM

The dual surface features of implants combining different surface roughness at the smooth transgingival part and roughened endosseous area can clearly be observed on the low-magnification SEM photomicrographs (Fig. 7a). Accordingly, FIB sections were performed at these locations, as shown in Fig. 7b and c. Monoclinic ZrO_2 grains with a typical twinning crystallographic contrast (chevron patterns) were found on the outer surface of CG implants (Fig. 7c). No evidence of post-processing procedures like sandblasting or acid etching was observed, in agreement with the fact that the implants were sintered subsequent to the injection moulding process. The implants were dense with only few micron-size pores occasionally observed. Microstructures at different locations on the implants were also uniform and consistent. The zirconia-grain size, measured from the linear-intercept method and then applying a correction factor of 1.56, was 0.55 ± 0.03 µm (95% confidence interval) with unimodal distributions.

After dynamic fatigue (cyclic loading and ageing), all positions showed a clear but very shallow (1–2 µm) transformation depth (Fig. 8a), in agreement with the XRD and µ-Raman measurements. FIB-sections at the internal smooth surface (implant-abutment connection) showed a similar depth of phase transformation (Fig. 8b). The depth of transformation zone was thus generally small, showing some micro-cracks running parallel to the surface.

4. Discussion

The implants were processed by ceramic injection-moulding (including the roughened surface). This manufacturing procedure effectively induced a surface roughness at the locations needed and monoclinic grains were only very scarcely observed at the surface of the non-loaded/non-aged CG implant. The phase composition with 13 vol% *m*-ZrO_2 is slightly higher than the monoclinic content found on other injection-moulded implants [51] but fulfils the ISO 13356 requirement of less than 20% *m*-ZrO_2 on as-received zirconia implants [31]. Note that the ISO 13356 however did not precisely define the limit of 20% in wt% or vol%. In any case, this small percentage of monoclinic content measured by XRD represents a very thin layer of transformation (about one grain-depth, as observed by FIB-SEM) after the overall process. The microstructure with grain size of about 0.55 µm are also typical in comparison to different one-piece 3Y-TZP ceramic implants [51]. Indeed, injection moulding did not alter the microstructure of zirconia ceramics, as opposed to other surface-roughening treatments like acid etching or laser patterning [53]. In general, the implants were also dense; only some isolated porosities were occasionally observed, as also observed for other commercially available zirconia implants manufactured by different methods [51]. XRD and µ-Raman revealed very limited amounts of monoclinic phase at the implant surface prior to loading/ageing, with different absolute values. The lower value obtained by µ-Raman compared to that recorded by XRD is a direct result of the increased penetration depth (20x of objective lens) of µ-Raman, estimated to be deeper than 20 µm, as compared to the penetration depth of XRD being about 5–7 µm; along with the fact that the aged-induced-transformation starts from the surface [54]. In other words, XRD is more sensitive, while µ-Raman with better lateral resolution (herein 4 µm) is useful to locally resolve the monoclinic phase content. The µ-Raman data were in agreement with the FIB-SEM results, showing that the injection moulding procedure resulted in a consistent and homogeneous microstructure and the same stability at different locations of the implants.

During the cyclic fatigue procedure, one implant failed after 4.7 million loading cycles. This is the first failure during chewing simulation in a series of comparable studies available in literature [20, 29]. A similar observation was made in an ongoing clinical trial [German Clinical Trials Register (DRKS) number DRKS00012469], running at Charité in Berlin and evaluating the same implant system. In this trial, one out of 25 implants fractured in a comparable manner in the region of a lower first molar at 182 days after loading (Fig. 9). The cause of fracture for this *in vivo* failed implant could not clearly be deduced from the fracture surface (Fig. 10a), but it is important to highlight that the fracture initiated from the bulk of the implant, analogous to the sample that fractured in the current *in vitro* cyclic fatigue test (Fig. 5c). X-ray tomography did not show a volume defect nor significant pores or flaws inside the implant (Fig. 10b), suggesting the need for further studies to fully understand the reason for implant failure during cyclic fatigue in this study and for the *in vivo* implant failure. After the cyclic loading/ageing procedure, the monoclinic ZrO_2 content at the implant surface increased significantly, however to a limited extent (36% of the superficial 5-7 µm XRD penetration depth, or 7% of the superficial 20 µm layer detected by µ-Raman), which is in accordance with the shallow 1–2 µm *t-m* transformation zone, as visualized by means of FIB-SEM in Fig. 8. As a result of cyclic loading with simultaneous ageing, the mean fracture load was significantly decreased by 244 N (≈ 20%). Considering that the highest bending moment clinically measured was 95 Ncm [55], additionally with a safety buffer of 100%, implants that were embedded according to ISO 14801 and withstood a fracture load of 200 Ncm, which approximately corresponds to 400 Ncm could be regarded as clinically safe. The implants that had survived the cyclic fatigue still revealed fracture load values satisfying clinical safety. Nevertheless, the decreased strength is in contrast to an earlier experiment with the same setup [29]. A likewise injection-moulded prototype zirconia implant was evaluated but was combined with a zirconia abutment. That prototype implant showed a comparable increase in

monoclinic phase content, but interestingly, fracture load increased after loading/ageing [29]. In such case, shallow ageing-induced-transformation with only few micro-cracks led to the compressive stress at the surface [41] and thereby increased the overall load-to-fracture, as also observed for several other implant systems [22]. For the present implant system, since loaded/aged OG implants were more deformed during the load-to-fracture test, also exhibiting a non-linear load-displacement curve (Fig. 4 and two videos in appendix), degradation of PEKK abutment might be the reason for the increased distortion and lowered overall fracture load. Zirconia ceramics, even aged, in general cannot deform in a non-linear way. However, the susceptibility to water/moisture-absorption of polymers [56-58], along which also amorphous PEEK, can significantly alter their mechanical properties and viscoelastic behaviour by inducing plasticization deformation or differential swelling strains [59, 60]. Water absorption takes place by diffusion or capillary processes, for which increased operational temperature even within a range of 5-60°C, higher water-vapour pressure and applied external stress can significantly accelerate the water-absorption kinetics [60, 61]. Although the abutment in this study was made from crystalline PEKK and not amorphous PEEK, the similarity between PEKK and PEEK along with the higher test temperature of 85°C with simultaneous cyclic loading allow us to speculate that the PEKK abutment may have been degraded/softened due to the imposed cyclic loading and ageing. When this would have happened, a non-linear deformation of the implant-abutment combination studied in this work can indeed be expected, thereby having changed the loading conditions and stress field of the zirconia implant so that it eventually fractured at a lower strength value. This assumption might also explain why fractures occurred at different locations/depth in zirconia for OG and CG implants, as shown in Figs. 5a and b. Evaluation of the hydrothermal degradation of the PEKK abutment however was not within the scope of the current manuscript but should definitely be explored further to elucidate the precise reasons for the

decreased strength recorded after cyclic loading and ageing. After all, the minimum fracture load of 493 N, as recorded in the present study after loading/ageing, can still be considered sufficient for clinical applicability, while the analysis of the failure mode and the reliability control of the zirconia implants investigated remain of major importance prior to clinical use. Note that regarding the sample for which the abutment screw and PEKK abutment fractured after 6.5 million loaded cycles, PEKK abutment was vertically fractured in the region of the internal abutment connection but it is unclear whether fracture of the screw or fracture of the abutment happened first. After the replacement of the screw and abutment, no difference was observed as compared with the samples that were cyclically loaded since the beginning of the test.

At last, the present study outcome highlights the need for adjusting the currently available standards to judge on clinical safety of implant systems. The experimental protocol in this work, involving cyclic fatigue in water at 85°C, has mimicked the oral environmental and chewing conditions to the best extent possible. After selecting the 1.5 mm supracrestal positioning of the implants, only the embedding procedure was adopted from the ISO 14801 standard, which prescribes to simulate a bone loss of 3 mm, apply the load 30° to the vertical axis, and use loading hemispheres resulting in a lever arm of 5.5 mm. While not required by this standard, the implants were also loaded by horizontal shear forces in a hot humid environment, liable to induce ageing of zirconia simultaneously with mechanical loading. The 10 million cycles applied in this work along with the 85°C hydrothermal treatment aimed to simulate 40 years of *in situ* ageing of zirconia-implant bodies in a given 60-day period, assuming an activation energy of 104 $kJ \cdot mol^{-1}$ for ageing [29, 41, 42]. Furthermore, this experimental procedure also does not match with the available ISO 13356 standard which suggests to test on polished quadrangular bars, while it is highly evidenced that different implant features and surface treatments can result in highly different ageing kinetics and

strength [22, 50, 62, 63]. The corresponding *in vitro* and *in vivo* results clearly highlight and validate the importance of pre-clinical experiments like the present one. Therefore, the adaptation and combination of two ISO 14801 and ISO 13356 standards, as applied in this work, can be proposed as laboratory test to check a priori the reliability of zirconia implants. Nevertheless, it is noteworthy that this protocol and the above discussed equivalence may not apply for the PEKK abutment, since the polymer-degradation mechanisms are different. Actually, it would be difficult or even impossible to simultaneously evaluate the performance of different materials in a complex system using *in vitro* study protocols, since the test conditions should be adjusted for each specific material following its respective degradation mechanisms. In the particular case of the present system, the potential degradation of PEKK properties following combined loading/ageing should be explored further in order to get insight into the PEKK degradation/softening mechanisms as well as the time-temperature equivalence to propose pertinent protocols and lifetime estimations.

5. Conclusions

The main outcome of this work can be summarised as follows:

- Injection moulding introduced dual micro-roughened surfaces as needed. Microstructure of typical 3Y-TZP zirconia ceramics and corresponding ageing susceptibility were consistent and homogeneous at different locations of the zirconia implants.
- Following the presented experimental setup, phase transformation was detectable but limited to a shallow transformation zone of ~2 µm at both internal and external surfaces of the implant system after hydrothermally induced ageing.
- The average fracture load of the evaluated implants before and after cyclic loading/ageing might be sufficient for clinical application. However, the mechanical resistance of

cyclically-loaded/aged implants was reduced, for which ageing of the zirconia implant is not considered responsible.

- The possible degradation/softening of the PEKK abutment and the potential impact on the present findings need to be investigated further. This degradation was likely the reason of the recorded decrease in failure load and the failure of one implant during cyclic fatigue.
- The presented findings emphasize the importance to adjust the standards for testing the reliability of zirconia-implant bodies and also suggest to adjust the test conditions for each specific material following its respective degradation mechanisms.

Declarations of interest

The authors state that there is no conflict of interest in this work.

CRediT authorship contribution statement

Fei Zhang: Formal analysis; Investigation; Methodology; Funding acquisition; Visualization; Writing - original draft; Writing - review & editing. **Christoph Meyer zur Heide:** Investigation; Writing - original draft. **Jérome Chevalier:** Formal analysis; Funding acquisition; Methodology; Writing - review & editing. **Jozef Vleugels:** Formal analysis; Methodology; Supervision; Writing - review & editing. **Christian Wesemann:** Investigation; Formal analysis. **Bernardo Camargo dos Santos:** Investigation; Writing - original draft; **Bart Van Meerbeek:** Supervision; Writing - review & editing. **Valter Sergo:** Funding acquisition; Writing - review & editing. **Kohal Ralf-Joachim:** Methodology; Writing - review & editing. **Erik Adolfsson:** Funding acquisition; Writing - review & editing. **Insa Herklotz:** Investigation (Clinical Failure). **Spies Benedikt:** Formal analysis; Investigation;

Methodology; Supervision; Funding acquisition; Visualization; Writing - original draft; Writing - review & editing.

Acknowledgements

The work was supported by a grant of the Oral Reconstruction Foundation (Reference: ORF21801) and by the Research Foundation - Flanders (FWO Vlaanderen) in light of F. Zhang's post-doctoral fellowship (12S8418N).

References

[1] P.I. Branemark, R. Adell, U. Breine, B.O. Hansson, J. Lindstrom, A. Ohlsson, Scand J Plast Reconstr Surg, 3 (1969) 81-100. doi:10.3109/02844316909036699.
[2] B.E. Pjetursson, D. Thoma, R. Jung, M. Zwahlen, A. Zembic, Clin Oral Implants Res, 23 Suppl 6 (2012) 22-38. doi:10.1111/j.1600-0501.2012.02546.x.
[3] K. Gotfredsen, A. Wiskott, G. Working, Clin Oral Implants Res, 23 Suppl 6 (2012) 238-241. doi:10.1111/j.1600-0501.2012.02549.x.
[4] S. Sandhaus, Inf Odontostomatol, 4 (1968) 19-24.
[5] R.V. McKinney, Jr., D.L. Koth, The Journal of prosthetic dentistry, 47 (1982) 69-84. doi:10.1016/0022-3913(82)90245-1.
[6] M. Andreiotelli, R.J. Kohal, Clinical implant dentistry and related research, 11 (2009) 158-166. doi:10.1111/j.1708-8208.2008.00105.x.
[7] N. Cionca, D. Hashim, A. Mombelli, Periodontology 2000, 73 (2017) 241-258. doi:10.1111/prd.12180.
[8] M. Andreiotelli, H.J. Wenz, R.J. Kohal, Clin Oral Implants Res, 20 Suppl 4 (2009) 32-47. doi:10.1111/j.1600-0501.2009.01785.x.
[9] R.J. Kohal, D. Weng, M. Bachle, J.R. Strub, Journal of periodontology, 75 (2004) 1262-1268. doi:10.1902/jop.2004.75.9.1262.
[10] R. Depprich, H. Zipprich, M. Ommerborn, C. Naujoks, H.P. Wiesmann, S. Kiattavorncharoen, H.C. Lauer, U. Meyer, N.R. Kubler, J. Handschel, Head & face medicine, 4 (2008) 30. doi:10.1186/1746-160X-4-30.
[11] H.J. Wenz, J. Bartsch, S. Wolfart, M. Kern, The International journal of prosthodontics, 21 (2008) 27-36.
[12] A. Scarano, F. Di Carlo, M. Quaranta, A. Piattelli, The Journal of oral implantology, 29 (2003) 8-12. doi:10.1563/1548-1336(2003)029<0008:BRTZCI>2.3.CO;2.
[13] S. Pieralli, R.J. Kohal, R.E. Jung, K. Vach, B.C. Spies, Journal of dental research, 96 (2017) 38-46. doi:10.1177/0022034516664043.
[14] C. Piconi, G. Maccauro, Biomaterials, 20 (1999) 1-25. doi:10.1016/S0142-9612(98)00010-6.
[15] J. Chevalier, Biomaterials, 27 (2006) 535-543. doi:10.1016/j.biomaterials.2005.07.034.
[16] J. Chevalier, L. Gremillard, S. Deville, Annual review of materials research, 37 (2007) 1-32. doi:10.1146/annurev.matsci.37.052506.084250.

[17] R.J. Kohal, J.B. Kilian, S. Stampf, B.C. Spies, Materials (Basel, Switzerland), 8 (2015) 1577-1589. doi:10.3390/ma8041577.
[18] F.H. Schunemann, M.E. Galarraga-Vinueza, R. Magini, M. Fredel, F. Silva, J.C.M. Souza, Y. Zhang, B. Henriques, Mater Sci Eng C Mater Biol Appl, 98 (2019) 1294-1305. doi:10.1016/j.msec.2019.01.062.
[19] I. Denry, J.R. Kelly, Dental materials : official publication of the Academy of Dental Materials, 24 (2008) 299-307. doi:10.1016/j.dental.2007.05.007.
[20] B.C. Spies, A. Fross, E. Adolfsson, A. Bagegni, S. Doerken, R.J. Kohal, Dental materials : official publication of the Academy of Dental Materials, 34 (2018) 1585-1595. doi:10.1016/j.dental.2018.08.290.
[21] B.C. Spies, C. Sauter, M. Wolkewitz, R.J. Kohal, Dental materials : official publication of the Academy of Dental Materials, 31 (2015) 262-272. doi:10.1016/j.dental.2014.12.013.
[22] M. Monzavi, F. Zhang, S. Meille, T. Douillard, J. Adrien, S. Noumbissi, H. Nowzari, J. Chevalier, Journal of the mechanical behavior of biomedical materials, 101 (2020) 103423. doi:10.1016/j.jmbbm.2019.103423.
[23] Y.S. Park, S.H. Chung, W.J. Shon, Clin Oral Implants Res, 24 (2013) 586-591. doi:10.1111/j.1600-0501.2012.02468.x.
[24] C. Piconi, S. Sprio, Current Oral Health Reports, 5 (2018) 186-193. doi:10.1007/s40496-018-0187-x.
[25] B.C. Spies, J. Nold, K. Vach, R.J. Kohal, Journal of the mechanical behavior of biomedical materials, 53 (2016) 1-10. doi:10.1016/j.jmbbm.2015.07.005.
[26] M. Payer, A. Heschl, M. Koller, G. Arnetzl, M. Lorenzoni, N. Jakse, Clin Oral Implants Res, 26 (2015) 371-376. doi:10.1111/clr.12342.
[27] F. Rahmitasari, Y. Ishida, K. Kurahashi, T. Matsuda, M. Watanabe, T. Ichikawa, Dent J (Basel), 5 (2017) 35. doi:10.3390/dj5040035.
[28] S.S. Atsu, M.E. Aksan, A.C. Bulut, The International journal of oral & maxillofacial implants, 34 (2019) 622-630. doi:10.11607/jomi.7036.
[29] B.C. Spies, M.E. Maass, E. Adolfsson, V. Sergo, T. Kiemle, C. Berthold, E. Gurian, S. Fornasaro, K. Vach, R.J. Kohal, Dental materials : official publication of the Academy of Dental Materials, 33 (2017) 954-965. doi:10.1016/j.dental.2017.06.002.
[30] ISO 14801, (2017-03) 1-15.
[31] ISO 13356, (2015-09) 1-12.
[32] J. Chevalier, J. Loh, L. Gremillard, S. Meille, E. Adolfson, Acta biomaterialia, 7 (2011) 2986-2993. doi:10.1016/j.actbio.2011.03.006.
[33] C. Sanon, J. Chevalier, T. Douillard, R.J. Kohal, P.G. Coelho, J. Hjerppe, N.R. Silva, Dental materials : official publication of the Academy of Dental Materials, 29 (2013) 389-397. doi:10.1016/j.dental.2013.01.007.
[34] S. Lettry, B.B. Seedhom, E. Berry, M. Cuppone, Bone, 32 (2003) 35-44. doi:10.1016/s8756-3282(02)00921-3.
[35] B. RILO, N. FERNÁNDEZ-FORMOSO, M.J. MORA, C. CADARSO-SUÁREZ, U. SANTANA, Journal of Oral Rehabilitation, 36 (2009) 571-576. doi:10.1111/j.1365-2842.2009.01956.x.
[36] H. Hayasaki, I. Saitoh, G.S. Throckmorton, Y. Iwase, S. Nakata, M. Nakata, Journal of Oral Rehabilitation, 30 (2003) 1041-1046. doi:10.1046/j.1365-2842.2003.01182.x.
[37] R. DeLong, R.L. Sakaguchi, W.H. Douglas, M.R. Pintado, Dental materials : official publication of the Academy of Dental Materials, 1 (1985) 238-242. doi:10.1016/S0109-5641(85)80050-6.

[38] R.L. Sakaguchi, W.H. Douglas, R. DeLong, M.R. Pintado, Dental materials : official publication of the Academy of Dental Materials, 2 (1986) 235-240. doi:10.1016/s0109-5641(86)80034-3.
[39] J.M. Po, J.A. Kieser, L.M. Gallo, A.J. Tesenyi, P. Herbison, M. Farella, Journal of dental research, 90 (2011) 1206-1210. doi:10.1177/0022034511416669.
[40] M. Rosentritt, M. Behr, R. Gebhard, G. Handel, Dental materials : official publication of the Academy of Dental Materials, 22 (2006) 176-182. doi:10.1016/j.dental.2005.04.024.
[41] F. Zhang, M. Inokoshi, K. Vanmeensel, B. Van Meerbeek, I. Naert, J. Vleugels, Acta Materialia, 92 (2015) 290-298. doi:10.1016/j.actamat.2015.04.001.
[42] J. Chevalier, B. Cales, J.M. Drouin, Journal of the American Ceramic Society, 82 (2004) 2150-2154. doi:10.1111/j.1151-2916.1999.tb02055.x.
[43] M. Keuper, C. Berthold, K.G. Nickel, Acta biomaterialia, 10 (2014) 951-959.
[44] V. Presser, M. Keuper, C. Berthold, K.G. Nickel, Applied spectroscopy, 63 (2009) 1288-1292. doi:10.1366/000370209789806975.
[45] N. Everall, J. Lapham, F. Adar, A. Whitley, E. Lee, S. Mamedov, Applied spectroscopy, 61 (2007) 251-259. doi:10.1366/000370207780220859.
[46] N. Djaker, C. Wulfman, M. Sadoun, M. Lamy de la Chapelle, Biomed Opt Express, 4 (2013) 725-731. doi:10.1364/BOE.4.000725.
[47] R.C. Garvie, P.S. Nicholson, Journal of the American Ceramic Society, 55 (1972) 303-305. doi:10.1111/j.1151-2916.1972.tb11290.x.
[48] H. Toraya, M. Yoshimura, S. Somiya, Journal of the American Ceramic Society, 67 (1984) C-119-C-121. doi:10.1111/j.1151-2916.1984.tb19715.x.
[49] J.A. Muñoz Tabares, M.J. Anglada, Journal of the American Ceramic Society, 93 (2010) 1790-1795. doi:10.1111/j.1551-2916.2010.03635.x.
[50] C. Sanon, J. Chevalier, T. Douillard, M. Cattani-Lorente, S.S. Scherrer, L. Gremillard, Dental materials : official publication of the Academy of Dental Materials, 31 (2015) 15-25. doi:10.1016/j.dental.2014.09.002.
[51] M. Monzavi, F. Zhang, T. Douillard, L. Gremillard, S. Noumbissi, H. Nowzari, J. Chevalier, Journal of the European Ceramic Society, 40 (2020) 3642-3655. doi:10.1016/j.jeurceramsoc.2020.03.050.
[52] M.I. MENDELSON, Journal of the American Ceramic Society, 52 (1969) 443-446. doi:10.1111/j.1151-2916.1969.tb11975.x.
[53] E. Roitero, F. Lasserre, J.J. Roa, M. Anglada, F. Mücklich, E. Jiménez-Piqué, Journal of the European Ceramic Society, 37 (2017) 4876-4887. doi:10.1016/j.jeurceramsoc.2017.05.052.
[54] J. Chevalier, L. Gremillard, A.V. Virkar, D.R. Clarke, Journal of the American Ceramic Society, 92 (2009) 1901-1920. doi:10.1111/j.1551-2916.2009.03278.x.
[55] T.R. Morneburg, P.A. Proschel, The International journal of prosthodontics, 16 (2003) 481-486.
[56] G. Baschek, G. Hartwig, F. Zahradnik, Polymer, 40 (1999) 3433-3441. doi:10.1016/s0032-3861(98)00560-6.
[57] C.-C.M. Ma, S.-W. Yur, Polymer Engineering and Science, 31 (1991) 34-39. doi:10.1002/pen.760310107.
[58] G. Mensitieri, A. Apicella, J.M. Kenny, L. Nicolais, Journal of Applied Polymer Science, 37 (1989) 381-392. doi:10.1002/app.1989.070370207.
[59] K.P. Pramoda, T. Liu, Journal of Polymer Science Part B: Polymer Physics, 42 (2004) 1823-1830. doi:10.1002/polb.20061.
[60] A. Raffaella, A. Antonio, American Journal of Engineering and Applied Sciences, 9 (2016) 565-573. doi:10.3844/ajeassp.2016.565.573.

[61] C.J. Wolf, H. Fu, Journal of Polymer Science Part B: Polymer Physics, 33 (1995) 331-332. doi:10.1002/polb.1995.090330219.
[62] M. Inokoshi, K. Vanmeensel, F. Zhang, J. De Munck, G. Eliades, S. Minakuchi, I. Naert, B. Van Meerbeek, J. Vleugels, Dental materials : official publication of the Academy of Dental Materials, 31 (2015) 182-194. doi:10.1016/j.dental.2014.11.018.
[63] M. Cattani-Lorente, S.S. Scherrer, S. Durual, C. Sanon, T. Douillard, L. Gremillard, J. Chevalier, A. Wiskott, Dental materials : official publication of the Academy of Dental Materials, 30 (2014) 1136-1146. doi:10.1016/j.dental.2014.07.004.

Tables

Table 1. Results of load-to-fracture.

Experimental group	Implant number	Mean ± SD (N)	95% confidence interval (N)	Characteristic fracture load[a] (N)
Observational Group (OG)	6	751 ± 231	936-556	831
Control Group (CG)	7	995 ± 161	1114-876	1062

a: failure probability of 63.2%.

Table 2: Monoclinic ZrO_2 phase content, as characterized by XRD and µ-Raman

		µ-Raman			Significance
	XRD	External smooth transgingival part	External roughened		
			Thread crest	Thread root	
OG (vol %)	36 ± 2	7 ± 1	6 ± 1	7 ± 3	$p = .931^b$ ($\eta^2 = .001$)
CG (vol%)	13 ± 2	2 ± 1	4 ± 2	2 ± 1	
Significance	$p < .001^a$	$p < .001^b$ ($\eta^2 = .145$)			

a: Uneaqual variances t-test (Welch-test) for XRD results; b: Multivariate linear regression model with the factors (implant group and position) for µ-Raman measurements.

Figure legends

Fig. 1. Sketch of the experimental design.

Fig. 2. The complementary phase characterization by XRD on the implant surface and by μ-Raman to locally resolve the monoclinic phase content on all CG and OG implants. A representative XRD pattern and μ-Raman spectrum are shown.

Fig. 3. Failure probability plot with 95% confidence bands of the fracture load for implants that survived the cyclic loading and ageing, compared to the control group.

Fig. 4. Load versus displacement recorded during load-to-fracture test. Average value (solid lines) and scattering (shaded areas) are shown in the image. Higher deformation was observed for the observational group implants that survived the cyclic loading and ageing (OG, loaded/aged; red line) as compared to the control group non-loaded/non-aged implants (CG, as received; blue line).

Fig. 5. Fractographic analysis for CG implants after load-to-fracture test (a), OG implants that survived the fatigue (cyclic loading and ageing) and fractured by load-to-fracture test (b), and OG implant that failed during fatigue (c). All failures occurred at the zirconia implant body part but initiated from different locations: (a) CG implants fractured from the inside from the implant-abutment interface and the tip of the Ti abutment screw was exposed due to fracture. (b) OG implants fractured from the outside of the zirconia implant and the Ti abutment screw was not exposed. (c) Implant No. 14 failed during cyclic fatigue with the failure initiated from the bulk of zirconia implant and the Ti screw was exposed.

Fig. 6. Box plot presenting the monoclinic ZrO_2 content as measured by µ-Raman before (CG, left plots) and after (OG, right plots) cyclic fatigue and ageing.

Fig. 7. FIB-SEM images of CG implants. (a) SEM surface images. (b) Exemplary images of FIB-sections located at the thread crest, thread root and smooth transgingival part. (c) FIB-SEM cross-sectional images.

Fig. 8. FIB-SEM cross-sectional images of OG implants. (a) External surfaces at positions analogous to those shown in Fig. 6b. (b) Internal surface at the implant-abutment connection.

Fig. 9. Clinical failure of the zirconia implant system used for the present study (same diameter, 182 days post loading) resulted in the need of an invasive surgical removal using a trephine bur.

Fig. 10. (a) SEM image of the fractured surface of the clinical failure shown in Fig. 9 (arrows indicate the fracture line). (b) X-ray tomography revealing absence of defects and porosities.

Appendix: Two representative videos recording the load-to-fracture process of two implants belonging to the CG (Nr. 7) and OG group (Nr. 11), respectively, showing the increased distortion of abutments of the OG implants.

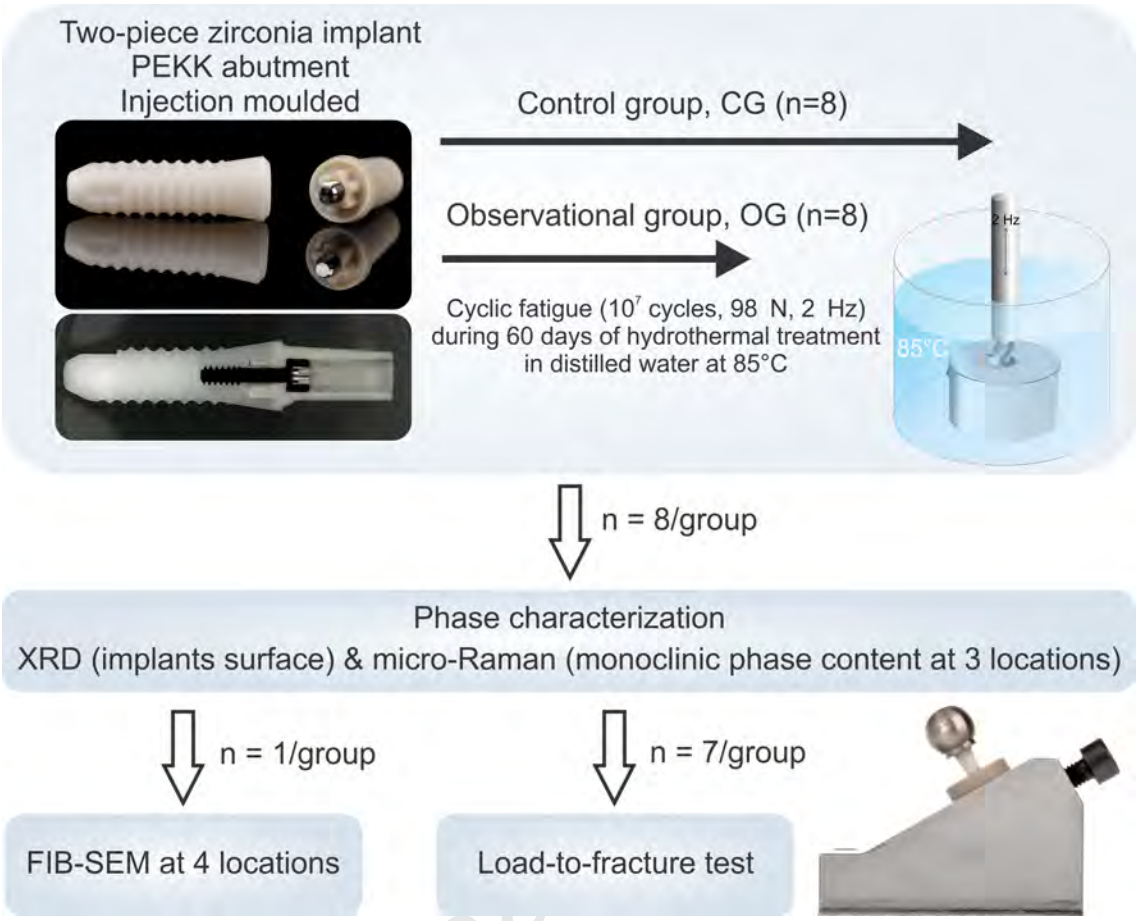
Two-piece zirconia implant
PEKK abutment
Injection moulded
Control group, CG (n=8)
Observational group, OG (n=8)
Cyclic fatigue (10^7 cycles, 98 N, 2 Hz)
during 60 days of hydrothermal treatment
in distilled water at 85°C
2 Hz
85°C
n = 8/group
Phase characterization
XRD (implants surface) & micro-Raman (monoclinic phase content at 3 locations)
n = 1/group
n = 7/group
FIB-SEM at 4 locations
Load-to-fracture test

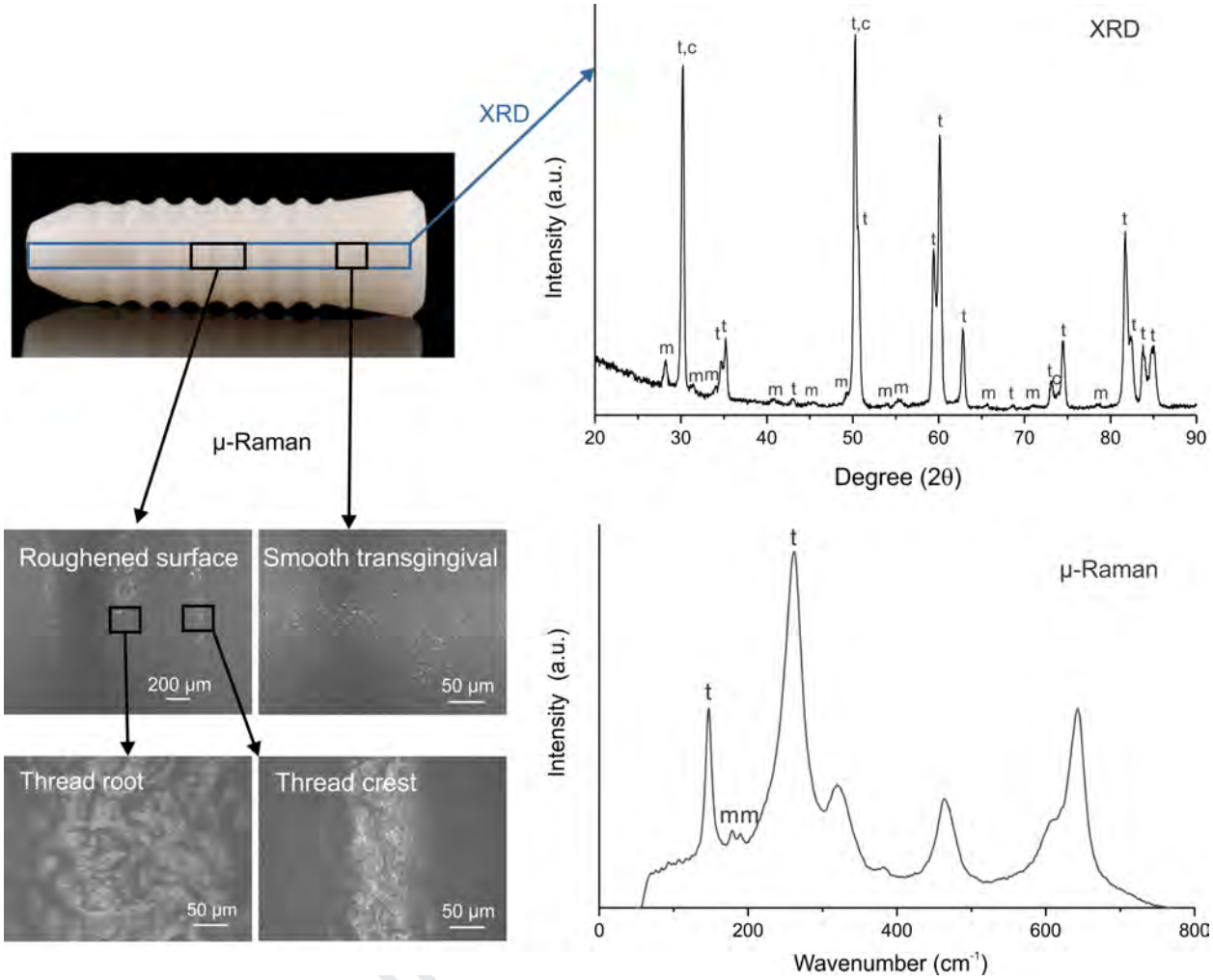
XRD
μ-Raman
Roughened surface
Smooth transgingival
200 μm
50 μm
Thread root
Thread crest
50 μm
50 μm
XRD
Intensity (a.u.)
Degree (2θ)
μ-Raman
Intensity (a.u.)
Wavenumber (cm-1)

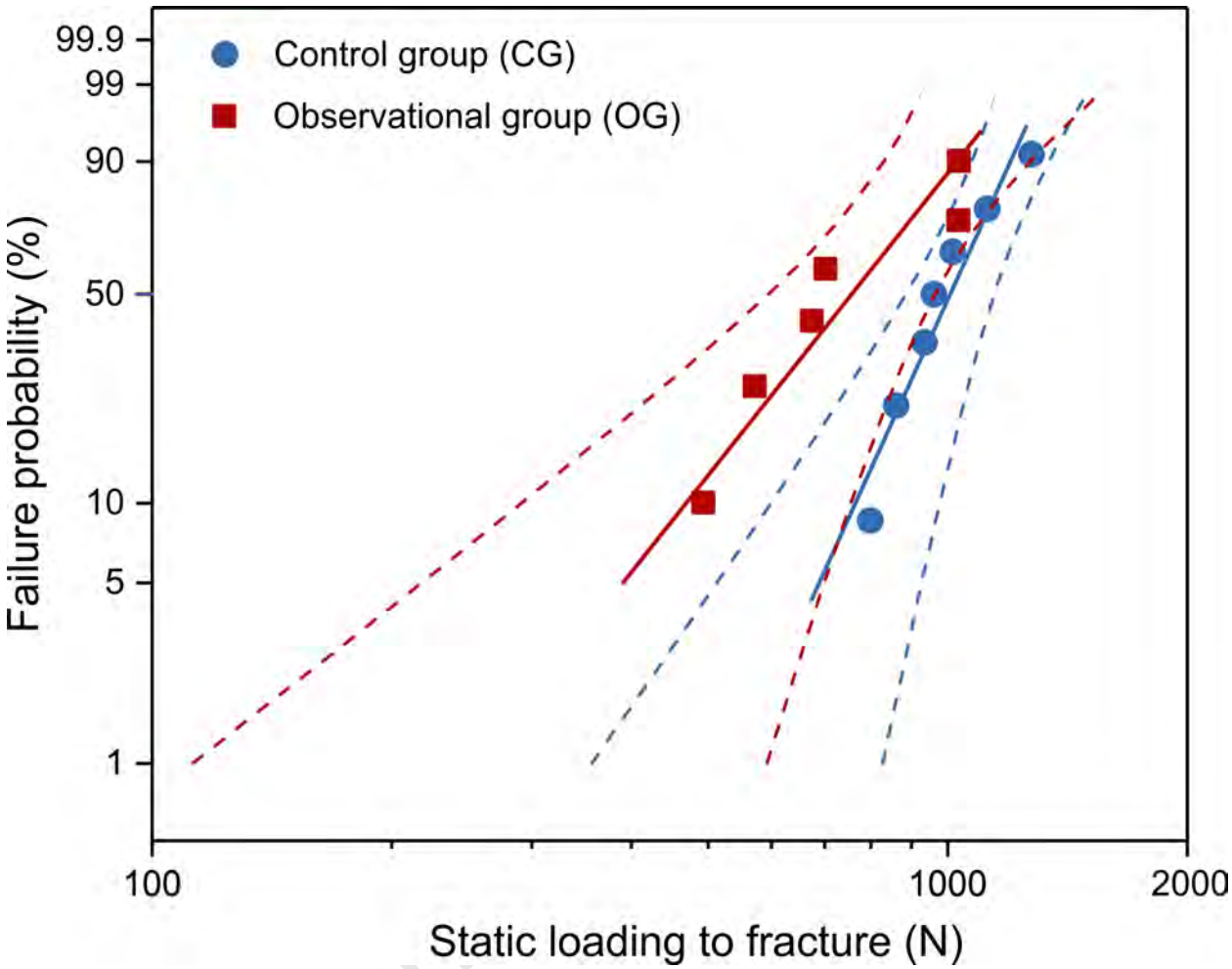
Control group (CG)
Observational group (OG)
Failure probability (%)
99.9
99
90
50
10
5
1
100
1000
2000
Static loading to fracture (N)

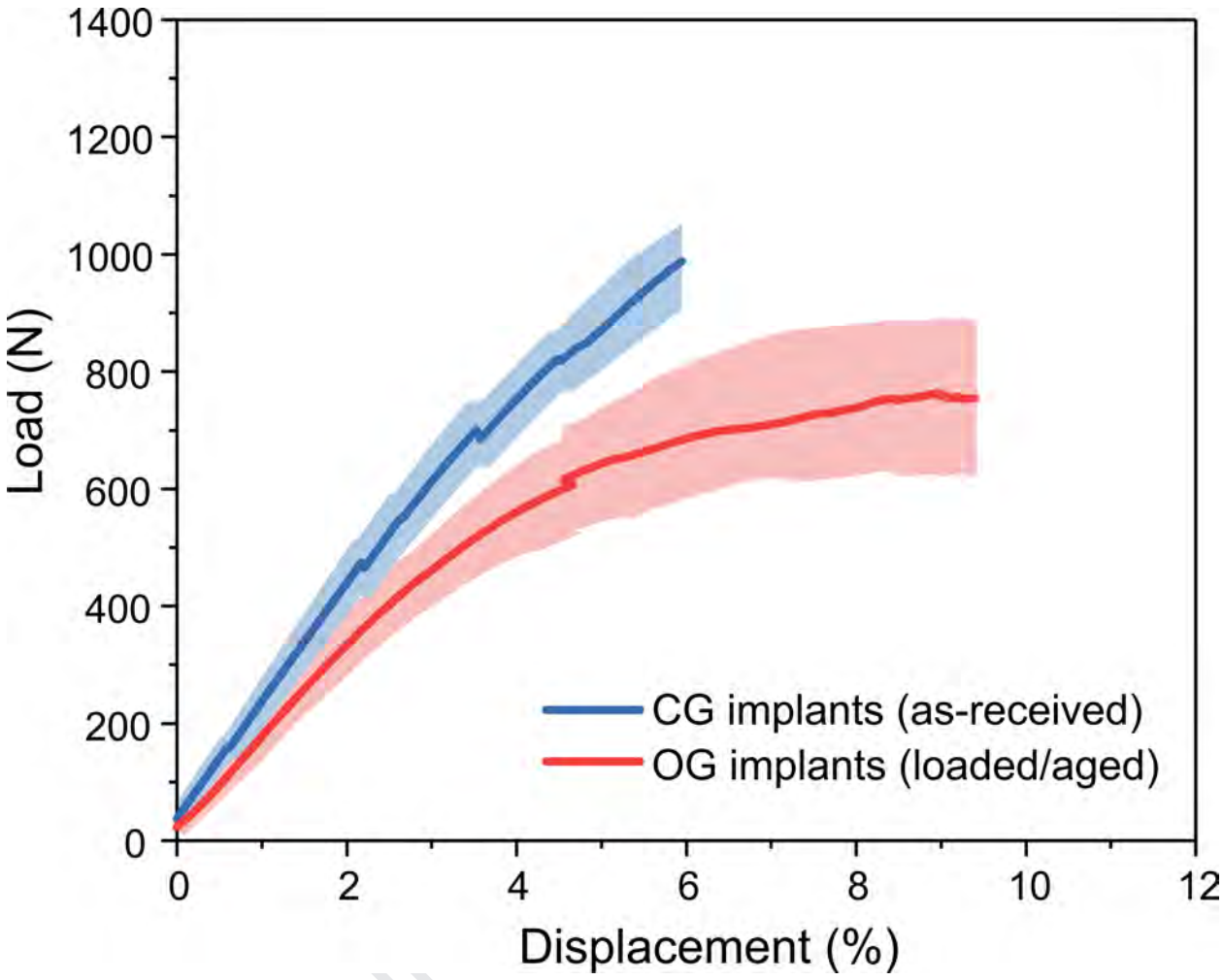
1400
1200
1000
800
600
400
200
0
Load (N)
0
2
4
6
8
10
12
Displacement (%)
CG implants (as-received)
OG implants (loaded/aged)

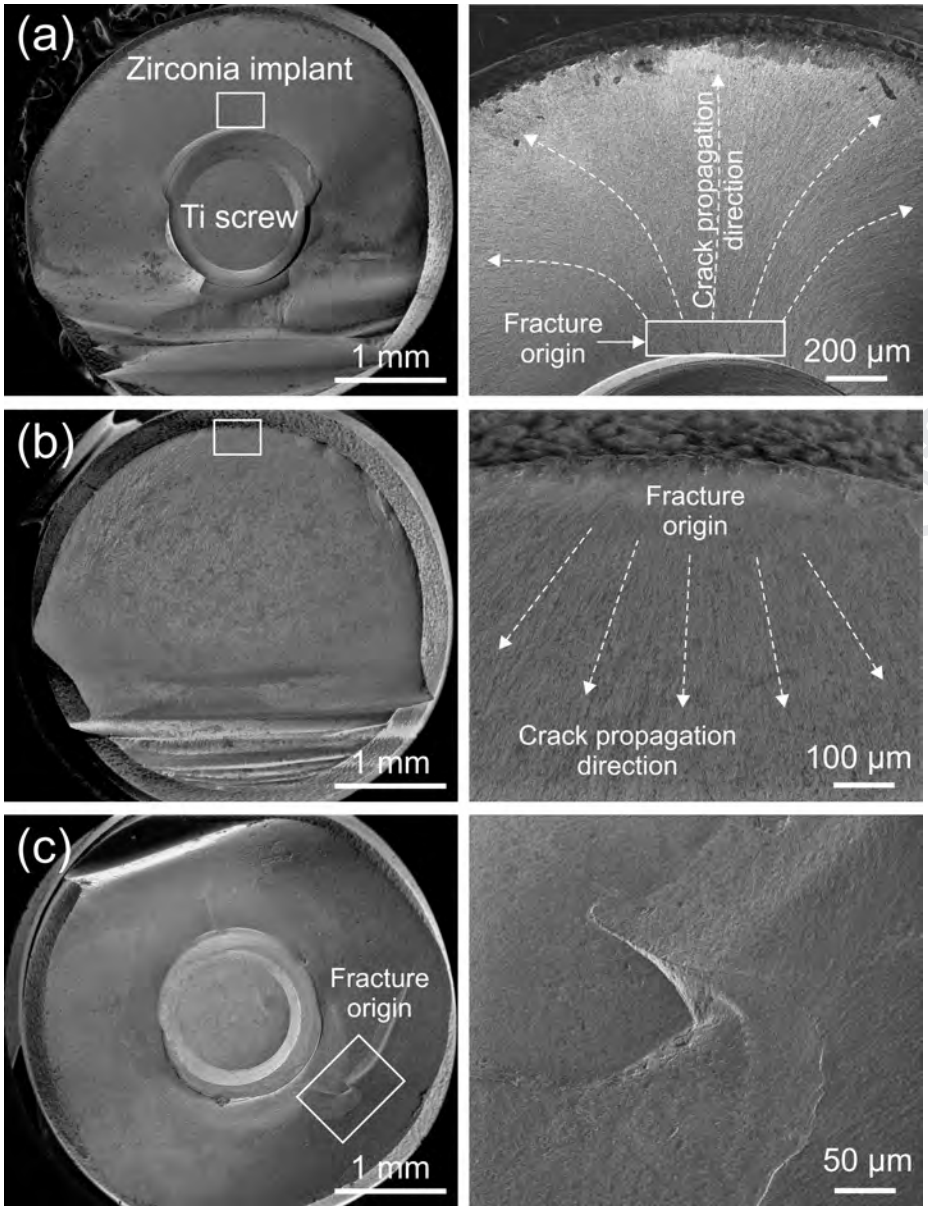
(a)
Zirconia implant
Ti screw
1 mm
Crack propagation direction
Fracture origin
200 μm
(b)
1 mm
Fracture origin
Crack propagation direction
100 μm
(c)
Fracture origin
1 mm
50 μm

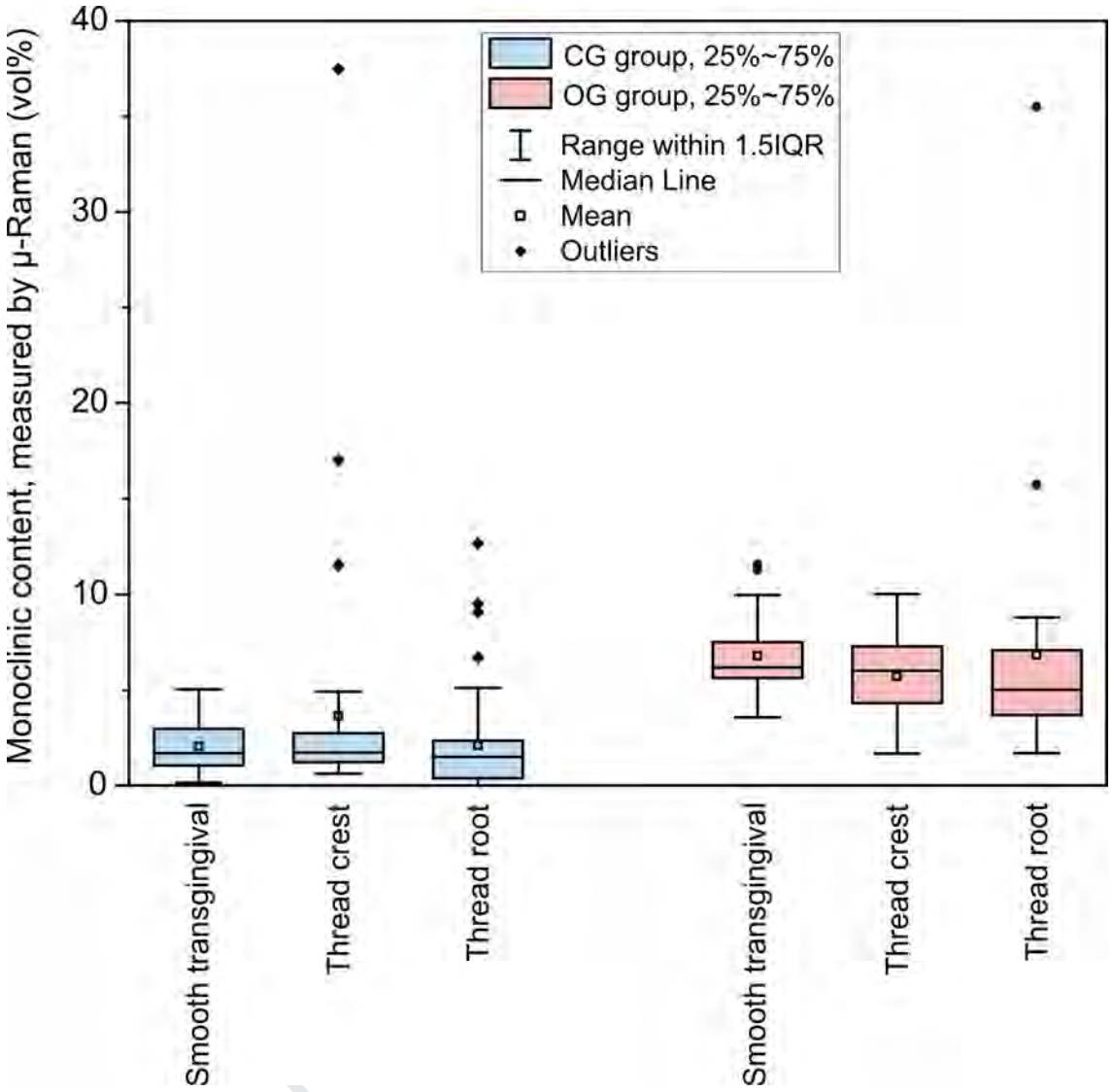
CG group, 25%~75%
OG group, 25%~75%
Range within 1.5IQR
Median Line
Mean
Outliers
Monoclinic content, measured by μ-Raman (vol%)
0
10
20
30
40
Smooth transgingival
Thread crest
Thread root
Smooth transgingival
Thread crest
Thread root

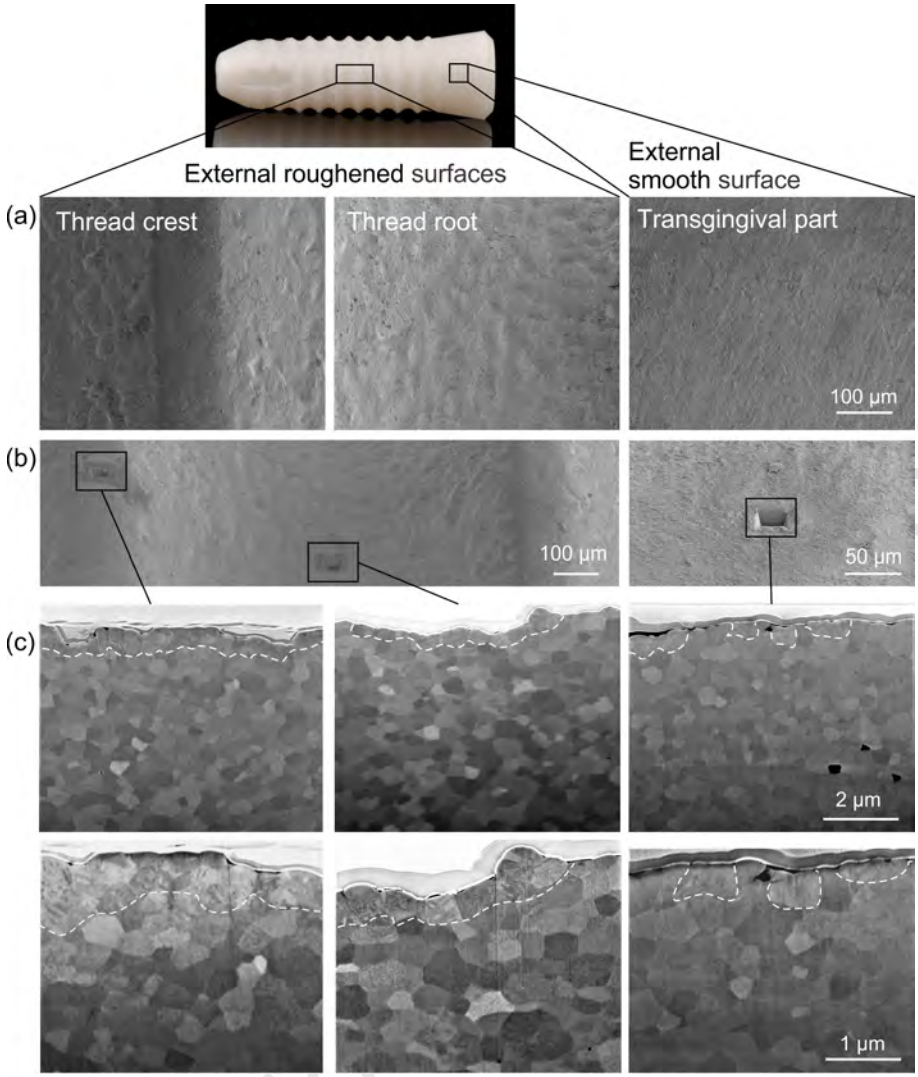
External roughened surfaces
External smooth surface
(a)
Thread crest
Thread root
Transgingival part
100 μm
(b)
100 μm
50 μm
(c)
2 μm
1 μm

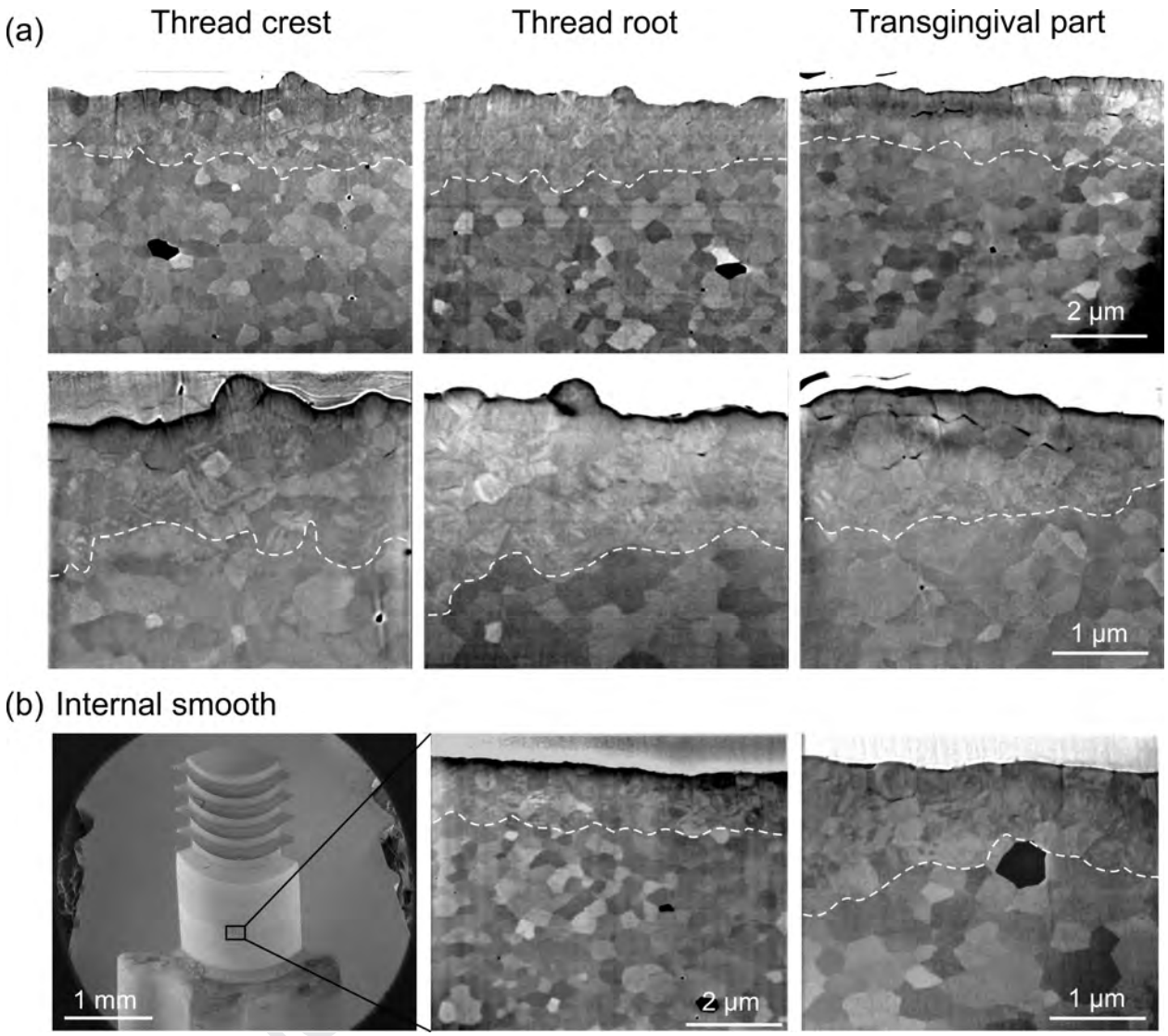
(a)
Thread crest
Thread root
Transgingival part
2 μm
1 μm
(b) Internal smooth
1 mm
2 μm
1 μm

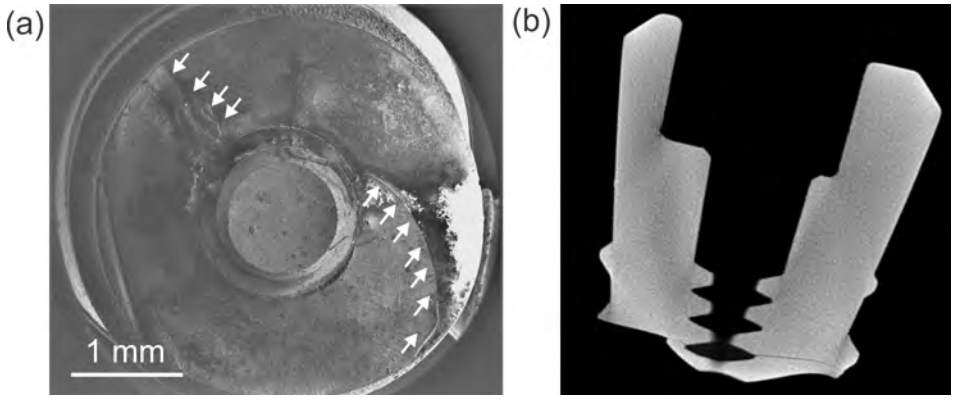

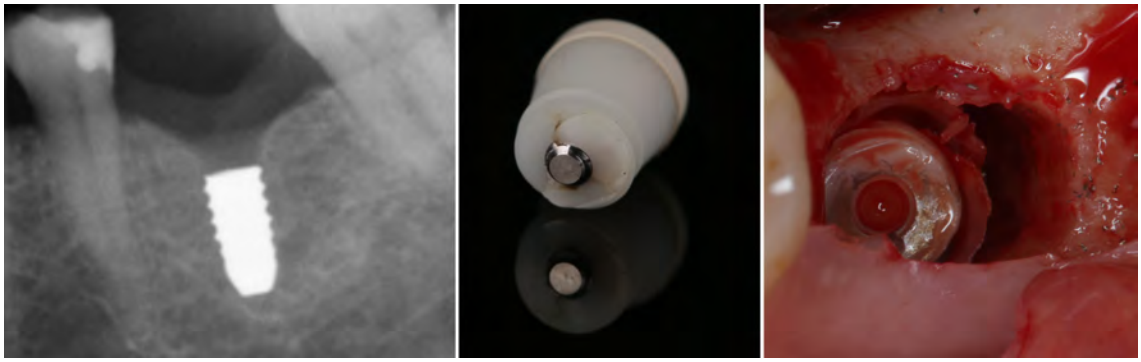

Highlights

- First study evaluating a two-piece, injection-moulded zirconia implant against PEKK abutment.
- Strength of the implants was sufficient for clinical application but affected by the long-term cyclic fatigue in the hydrothermal environment.
- The loading/ageing combination had a limited impact on the zirconia component itself, but more pronounced on the PEKK abutment.
- Tests were based on the adaptation of two ISO standards: ISO 14801 and ISO 13356. A combination of these standards may be proposed to check a priori the reliability of zirconia-based implants.
- Further research is needed to address the potential degradation of PEKK under cyclic fatigue in humid environment.

Declaration of interest

The authors state that there is no conflict of interest in this work.